ACS APPLIED MATERIALS & INTERFACES

Research Article

www.acsami.org

An In Situ Ionic-Liquid-Assisted Synthetic Approach to Iron Fluoride/Graphene Hybrid Nanostructures as Superior Cathode Materials for Lithium Ion Batteries

Bingjiang Li,[‡] David W. Rooney,[§] Naiqing Zhang,*[,†,‡] and Kening Sun*[,†,‡]

[†]State Key Laboratory of Urban Water Resource and Environment, Harbin Institute of Technology, Harbin, Heilongjiang, 150090, China

[‡]Academy of Fundamental and Interdisciplinary Sciences, Department of Chemistry, Harbin Institute of Technology, Harbin, 150001, China

[§]School of Chemistry and Chemical Engineering/QUILL Research Centre, Queen's University, Belfast, BT9 5AG, Northern Ireland, U.K.

Supporting Information

ABSTRACT: A tactful ionic-liquid (IL)-assisted approach to *in situ* synthesis of iron fluoride/graphene nanosheet (GNS) hybrid nanostructures is developed. To ensure uniform dispersion and tight anchoring of the iron fluoride on graphene, we employ an IL which serves not only as a green fluoride source for the crystallization of iron fluoride nanoparticles but also as a dispersant of GNSs. Owing to the electron transfer highways created between the nanoparticles and the GNSs, the iron fluoride/GNS hybrid cathodes exhibit a remarkable improvement in both capacity and rate performance (230 mAh g^{-1} at 0.1 C and 74 mAh g^{-1} at 40 C). The stable adhesion of iron fluoride nanoparticles on GNSs also introduces a significant improvement in long-term cyclic performance (115 mAh g^{-1} after 250 cycles even at 10 C). The superior electrochemical performance of these iron fluoride/GNS hybrids as lithium ion battery cathodes is ascribed to the robust structure of the hybrid and the synergies between iron fluoride nanoparticles and graphene.

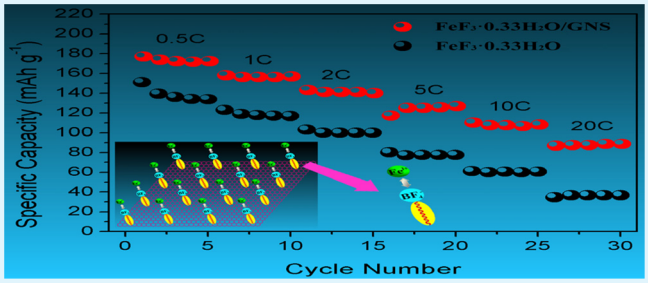

KEYWORDS: *graphene, high rate, ionic liquid, iron fluoride, lithium ion batteries*

INTRODUCTION

The demand for lithium ion battery (LIB) systems with high capacity and high power has grown at an unprecedented rate over the past decade.[1,2] While a lot of attention has been paid recently to high performance anodes, much less effort was placed for the development of efficient cathodes. $LiCoO_2$ and $LiFePO_4$ materials being used in cathodes of commercial LIBs currently have a low capacity (<170 mAh g^{-1}),[3−5] which leads to a restricted energy output. To realize LIBs with higher power and energy densities, exploring new cathode materials is urgently needed. Iron trifluoride has attracted a rapidly increasing amount of attention because of its high operating potential, high theoretical capacity of 237 mAh g^{-1}, abundant sources, and relatively low cost.[6−8] Despite these advantages, the use of iron trifluoride has been limited due to intrinsic drawbacks, for instance, the slow diffusion of Li^+ and low electron conductivity.

Constructing novel nanostructures is an alternative approach to address these problems.[9−13] For example, Maier and coworkers reported a nanoscale $FeF_3{\cdot}0.33H_2O$ material with an unusual tunnel structure.[14−16] This tunnel structure is beneficial for electrolyte penetration, Li ion transport, and interfacial processes. To further improve the power density of the iron trifluoride, various endeavors have been made to overcome the drawbacks by hybridizing iron trifluoride with a conductive additive phase (such as a polymerization coating or CNTs), which provides a facile electron pathway.[10,13,16] Compared with CNTs, graphene is a two-dimensional atom monolayer carbon and has outstanding mechanical properties and electron conductivity.[17−22] Other superiorities of graphene include high surface area for better interfacial contact and low fabricating cost compared to CNTs.[18,23] Thus, graphene may be a desired conductive building unit for hybridizing iron fluoride. Recently, Kung et al. reported the synthesis of a FeF_3/graphene composite paper through a photothermal-assisted strategy after mixing FeF_3 and GO.[24] In Kung's work, they first synthesized FeF_3 nanoparticles by a precipitation approach and then mixed FeF_3 powder and GO in solution to obtain the FeF_3/graphene composite. Thus, the FeF_3 nanoparticles are simply adsorbed onto the GO. The as-prepared FeF_3/graphene

Received: March 9, 2013
Accepted: May 20, 2013
Published: May 20, 2013

Scheme 1. The Synthesis Procedure of the $FeF_3{\cdot}0.33H_2O$/GNS Hybrid

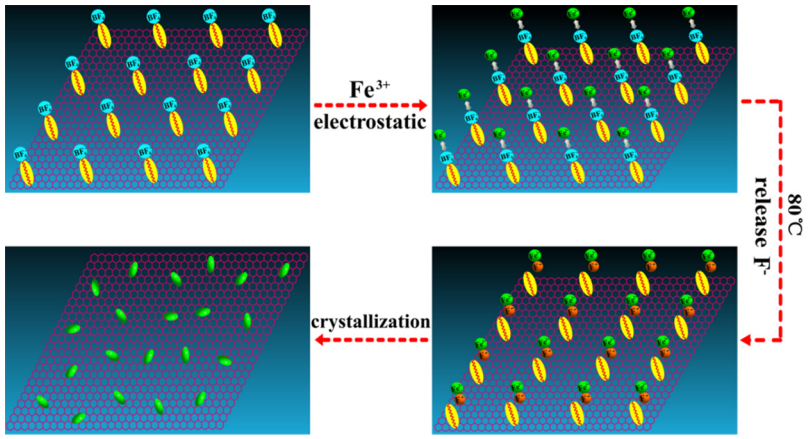

cathode showed a high energy density. However, the high rate performance and cycling stability of the material required improvement. This can be partly ascribed to the sample prepared by the *ex situ* method which would induce poor conductive contact between FeF_3 and the graphene nanosheets (GNSs). Consequently, a facile *in situ* approach for the synthesis of FeF_3/GNS hybrid nanostructures with robust stability and homogeneity is of great importance.

In this work, we developed a tactful ionic-liquid-assisted approach to *in situ* synthesize $FeF_3{\cdot}0.33H_2O$/GNS hybrid nanostructures in order to enhance the high-rate cycling performance. Herein, [Bmim][BF_4] (1-butyl-3-methylimidazolium tetrafluoroborate) ionic liquid (IL) was employed not only as a green fluoride source instead of the erosive HF, which was usually used as a fluoride source in previous reports,[10−13,25] but also served as a dispersant of GNSs. GNSs were chosen as the starting materials instead of graphene oxide (GO), thus avoiding additional reductive treatment to obtain GNSs from GO, which will easily cause destruction to the structure of FeF_3.[12,24] The π-cation interactions between the imidazolium cation of the [Bmim][BF_4] and the π-electrons of the GNSs promote the dispersion of GNSs in IL solution.[26−29] To our best knowledge, the obtained $FeF_3{\cdot}0.33H_2O$/GNS hybrid exhibits the best performance in high-rate capacity and long-term cycling stability reported in the literature. The $FeF_3{\cdot}0.33H_2O$/GNS hybrid nanostructure endows a steady and highly reversible specific capacity of more than 200 mAh g^{-1} even after 35 cycles and a good high-rate performance of 115 mAh g^{-1} even at a high current density of 2 A g^{-1} (10 C) after a long-term cycling of 250 cycles, which creates new chances in the development of high performance next-generation LIBs.

RESULTS AND DISCUSSION

The strategy used herein to synthesize the $FeF_3{\cdot}0.33H_2O$/GNS hybrid cathodes involves a three-step procedure which is schematically illustrated in Scheme 1. The procedure begins with the dispersion of the GNSs assisted by the IL *via* interactions between the imidazolium cation group of the IL and the π-electrons of graphene (1).[26−29] This is subsequently followed by the electrostatic attraction of the BF_4^- group of the IL with the Fe^{3+} (2). When heated, the BF_4^- group can release F^-, which acts as a fluoride source.[30,31] Subsequently, Fe^{3+} reacts with F^-, resulting in the *in situ* crystallization of iron trifluoride on the GNSs to obtain the hybrids (3). In this synthesis procedure, IL serving as a green fluoride source is operationally safe and environmentally friendly compared with erosive HF. Meanwhile, the cooperative interactions between the IL and the graphene lead to good dispersion of GNSs and the anchoring of $FeF_3{\cdot}0.33H_2O$ on the graphene.

The X-ray diffraction (XRD) patterns of the $FeF_3{\cdot}0.33H_2O$ and $FeF_3{\cdot}0.33H_2O$/GNS hybrid are compared in Figure 1. As

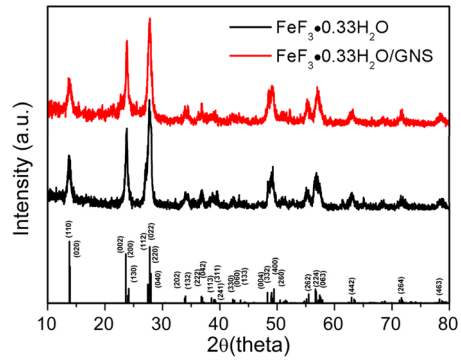

Figure 1. XRD patterns of $FeF_3{\cdot}0.33H_2O$ and $FeF_3{\cdot}0.33H_2O$/GNS.

shown in Figure 1, the X-ray diffraction peaks can be unambiguously assigned to hexagonal-tungsten-bronze-type $FeF_3{\cdot}0.33H_2O$ (JCPDS card no. 76-1262). Due to the small ratio of GNSs added, no carbon signals are detected.[16] The elemental analysis demonstrates that the carbon content in the hybrid is about 9 wt %.

The microstructure of the $FeF_3{\cdot}0.33H_2O$/GNS hybrid was characterized by TEM. Figure 2a illustrates that well-crystallized $FeF_3{\cdot}0.33H_2O$ nanoparticles are adhered firmly on the graphene layer and/or enclosed between the GNSs. The TEM image at high magnification in Figure 2b reveals the as-prepared $FeF_3{\cdot}0.33H_2O$/GNS hybrid. The $FeF_3{\cdot}0.33H_2O$ nanoparticles are distributed and tightly anchored on the graphene layers. Both the nucleation and crystallization of $FeF_3{\cdot}0.33H_2O$ nanoparticles occurred on the surface of GNSs. It is a typical one-pot and *in situ* method. Therefore, better contact will be realized between $FeF_3{\cdot}0.33H_2O$ and GNS.[18,19] Even after 20 min of ultrasonic treatment during the sample preparation for TEM characterization, the nanoparticles are still adhered firmly on GNSs.

As shown in Figure 2c, the $FeF_3{\cdot}0.33H_2O$ particles are anchored to the surface of the GNSs, which helps to prevent them from agglomeration and ensures a good dispersion over

dx.doi.org/10.1021/am400873e | ACS Appl. Mater. Interfaces 2013, 5, 5057−5063

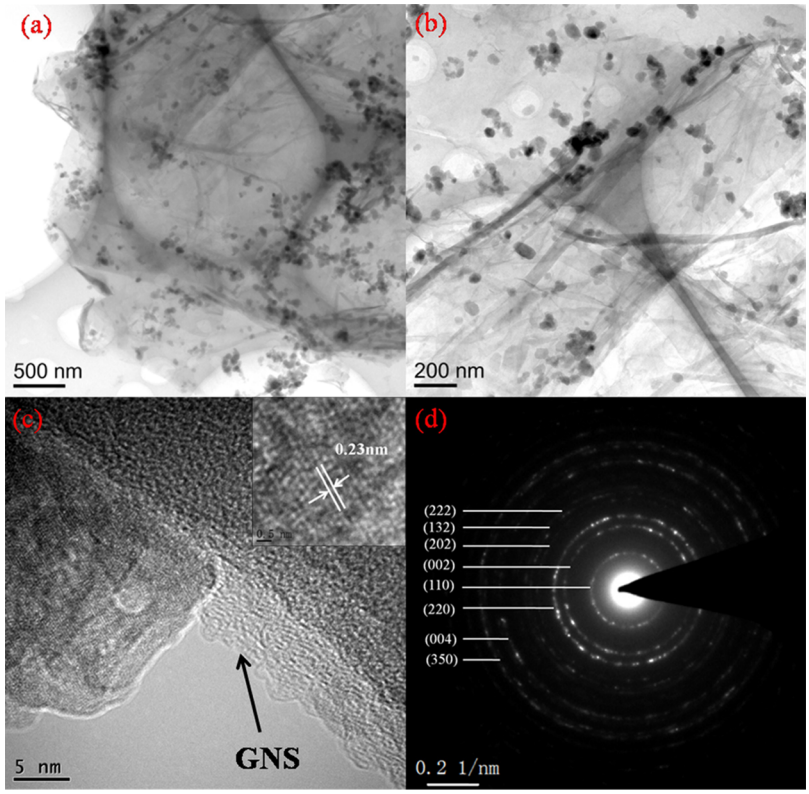

Figure 2. (a) TEM image of the $FeF_3{\cdot}0.33H_2O$/GNS hybrid, (b) high magnification TEM image of the $FeF_3{\cdot}0.33H_2O$/GNS hybrid, (c) high-resolution TEM images of the $FeF_3{\cdot}0.33H_2O$/GNS hybrid (the inset high-resolution TEM image shows clear lattices of $FeF_3{\cdot}0.33H_2O$ nanoparticles), and (d) SAED pattern of the $FeF_3{\cdot}0.33H_2O$/GNS hybrid.

the graphene support.[32−34] The lattice fringe of ∼0.23 nm is consistent with the (311) atomic planes of the $FeF_3{\cdot}0.33H_2O$. In addition, selected area electron diffraction analysis (SAED) of the $FeF_3{\cdot}0.33H_2O$/GNS hybrid confirms the polycrystalline structure of $FeF_3{\cdot}0.33H_2O$ nanoparticles. It is worth noting that only agglomerates of nanoparticles were formed without graphene (shown in Figure S1, Supporting Information). This result demonstrates that graphene plays a crucial role in the formation of well-dispersed $FeF_3{\cdot}0.33H_2O$ nanoparticles.

Raman spectroscopy is a forceful means to investigate the modification of graphene and their derivatives.[35,36] The Raman spectra of $FeF_3{\cdot}0.33H_2O$/GNS and GNSs shown in Figure 3 exhibit the regular two peaks, corresponding to the D-band line (ca. 1340 cm^{-1}) and the G-band line (ca. 1590 cm^{-1}),

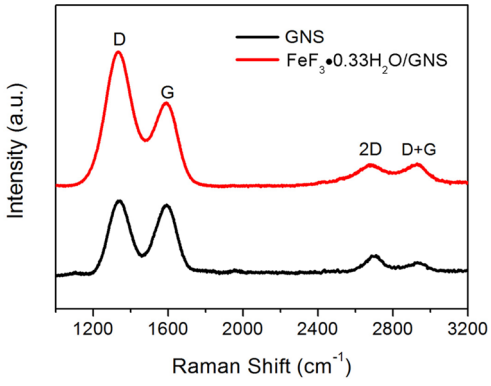

Figure 3. Raman spectra of the $FeF_3{\cdot}0.33H_2O$/GNS hybrid and GNSs.

respectively. The D-band is caused by edges or structural defects which can break the selection rule and symmetry; the G-band can be attributed to the first-order scattering of the sp^2 carbon domains.[35−38] The broadening 2D band (ca. 2680 cm^{-1}) confirms the multilayer structure of GNSs.[16,36,39,40] As shown, the I_D/I_G value of the hybrid is bigger than that of GNSs. The increased I_D/I_G indicates that the $FeF_3{\cdot}0.33H_2O$ nanoparticles lead to the increased disorder of graphene layers.[41,42]

The Brunauer−Emmett−Teller (BET) specific surface area and pore size distribution of the $FeF_3{\cdot}0.33H_2O$/GNS hybrid were measured by nitrogen isothermal adsorption (shown in Figure S2, Supporting Information). The BET specific surface area of the hybrid is 118 $m^2\ g^{-1}$, which can provide more reaction sites and is beneficial for electrolyte access. The sample exhibits a pore size distribution centered at 10 nm. This unique mesoporosity between the nanoparticles and GNSs may promote the diffusion of electrolyte ions, suggesting that the $FeF_3{\cdot}0.33H_2O$/GNS hybrid may show a large specific capacity and good high-rate performance.[19,43,44]

The electrochemical performance of the $FeF_3{\cdot}0.33H_2O$/GNS hybrid was evaluated by a discharge/charge test. In Figure 4, the discharge capacity during the first cycle achieved 230 mAh g^{-1}, and approximately corresponds to the insertion of 1.1 Li per formula. During discharging, the profiles show sloped reaction plateaus at 2.7 V which stem from the Li^+ insertion into the $FeF_3{\cdot}0.33H_2O$ forming the single-phase solid solution $Li_xFeF_3{\cdot}0.33H_2O$.[11,15,16] This typical Li-insertion reaction has been widely recognized by researchers through XRD characterization of the electrodes at various reaction stages.[15,45] On the contrary, extraction of Li from $Li_xFeF_3{\cdot}0.33H_2O$ forms

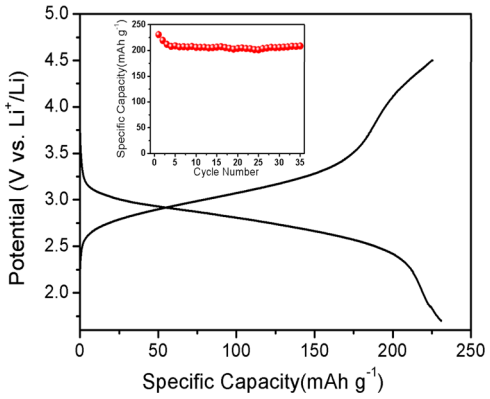

Figure 4. Voltage vs capacity profiles of the $FeF_3{\cdot}0.33H_2O$/GNS electrode during the first cycle. The inset is the cyclic performance of $FeF_3{\cdot}0.33H_2O$/GNS at 0.1 C.

$FeF_3{\cdot}0.33H_2O$ during charging. The cyclic performance of the $FeF_3{\cdot}0.33H_2O$/GNS electrode at 0.1 C is shown in the inset of Figure 4. The excess capacities during the initial cycles can be attributed to the reaction of functional groups on graphene with lithium ions and ion adsorption.[16,46,47] After 35 cycles, the electrodes still maintain a stable capacity over 200 mAh g^{-1}. It is worth noting that the hydrated water in $FeF_3{\cdot}0.33H_2O$ is indispensable, as it serves as a structural stabilizer.[11,15] The cycling stability demonstrates sufficient stability of hydrated water in the fluoride lattices, and the insertion/extraction process of Li^+ is quite reversible.

To evaluate the superiority of the hybrid for cathode materials, the electrochemical performances of the hybrid and bare $FeF_3{\cdot}0.33H_2O$ particles were compared in Figure 5. The discharge capacities at 0.5−40 C rates were compared in Figure 5a. As illustrated, the $FeF_3{\cdot}0.33H_2O$/GNS hybrid electrode shows a higher rate capability than the bare $FeF_3{\cdot}0.33H_2O$ electrode. The bare $FeF_3{\cdot}0.33H_2O$ electrode shows a specific capacity of 53 mAh g^{-1} at 10 C, reaching 40% of the initial capacity (132 mAh·g^{-1}) at 0.5 C. However, the $FeF_3{\cdot}0.33H_2O$/GNS electrode can yield 113 mAh·g^{-1} at 10 C with a capacity retention of 65% compared to that at a rate of 0.5 C. It is worth noting that the $FeF_3{\cdot}0.33H_2O$/GNS electrode can deliver 74 mAh·g^{-1} even at a discharge rate as high as 40 C (8 A g^{-1}).

To further highlight the effectiveness of graphene modification on improving the electrochemical performance of the material, the rate cycling performance is shown in Figure 5b. The hybrid illustrates much better rate performance. In particular, the $FeF_3{\cdot}0.33H_2O$/GNS hybrid still can deliver 89 mAh g^{-1} even at 4 A g^{-1} (20 C), i.e., 50% of the initial capacity. In a sharp contrast, the capacities of the bare $FeF_3{\cdot}0.33H_2O$ particles drop dramatically, with only 24% capacity remaining at the same rate. The increase of capacity is particularly obvious at higher rates for the hybrid. For example, at 20 C, the capacity of the $FeF_3{\cdot}0.33H_2O$/GNS hybrid is 89 mAh g^{-1}, which is 3 times more than that of the bare one. These results indicate that the unique hybrid nanostructures designed here are suitable for fast charging and discharging.

The small discharge capacity of GNSs between 4.5 and 1.7 V (less than 50 mAh g^{-1}) and the low content of GNSs in the hybrid (about 9 wt %) have little effect on the Li insertion/extraction process in our work. Hence, it is important to note that there is a strong synergistic effect between $FeF_3{\cdot}0.33H_2O$ nanoparticles and GNSs in the hybrid.[48,49] GNSs supply a large contact area for the $FeF_3{\cdot}0.33H_2O$ nanoparticles and serve as a remarkable conductive network to supply an expressway for

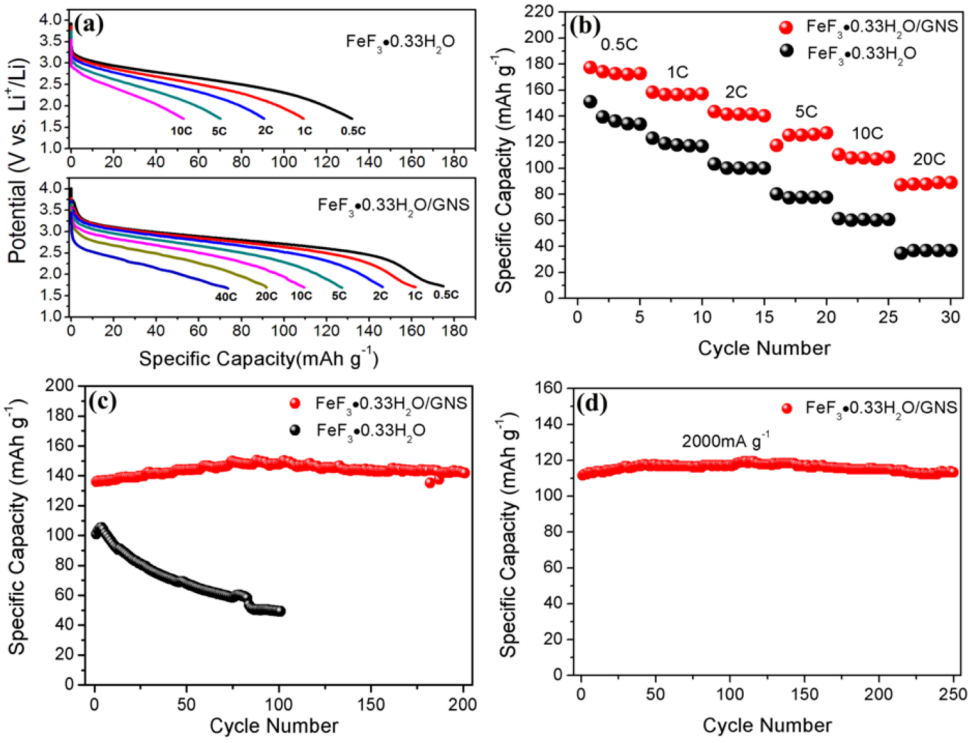

Figure 5. (a) Discharge profiles at different current rates, (b) rate cycling performance at different rates for the $FeF_3{\cdot}0.33H_2O$/GNS hybrid and bare $FeF_3{\cdot}0.33H_2O$, (c) cyclic performance of the $FeF_3{\cdot}0.33H_2O$/GNS hybrid and bare $FeF_3{\cdot}0.33H_2O$ at 1 C, and (d) cyclic performance of the $FeF_3{\cdot}0.33H_2O$/GNS hybrid at 10 C rate.

dx.doi.org/10.1021/am400873e | ACS Appl. Mater. Interfaces 2013, 5, 5057−5063

electron transfer. The strong anchoring of $FeF_3{\cdot}0.33H_2O$ nanoparticles on GNSs empowers fast electron transport through graphene layers to $FeF_3{\cdot}0.33H_2O$ particles to enhance the electrochemical performance. On the other hand, the anchoring particles on the GNSs can serve as spacers to prevent the restacking of GNSs, avoiding/weakening the decrease of the active specific surface area. Therefore, the synergistic effect of the $FeF_3{\cdot}0.33H_2O$ nanoparticles and graphene build an effective nanostructure for energy transmission and storage.

Figure 5c shows the cyclic performance of the bare $FeF_3{\cdot}0.33H_2O$ particles and $FeF_3{\cdot}0.33H_2O$/GNS hybrid at 1 C for 200 cycles. The specific capacities of the bare $FeF_3{\cdot}0.33H_2O$ particles decrease from 101 to 49 mAh g^{-1}. In sharp contrast, the $FeF_3{\cdot}0.33H_2O$/GNS hybrid still preserves a high stability, and in fact, its specific capacity increases from 136 to 142 mAh g^{-1} gradually (reaching the maximum 150 mAh g^{-1} after 100 cycles). Remarkably, the $FeF_3{\cdot}0.33H_2O$/GNS hybrid displays outstanding cyclic performance, and maintains a capacity of 115 mAh g^{-1} (~100 mAh g^{-1} when cycled between 2 and 4.5 V) without any decrease after 250 cycles even at 2 A g^{-1} (Figure 5d). The $FeF_3{\cdot}0.33H_2O$ nanoparticles anchored firmly on the GNSs, which are formed through the *in situ* crystallization in the $FeF_3{\cdot}0.33H_2O$/GNS hybrid nanostructures, ensure the high reversible capacity and long cyclic stability at high current density.

To explain the oustanding electrochemical performance of $FeF_3{\cdot}0.33H_2O$/GNS, the electrochemical impedance spectroscopy (EIS) was applied before cycling and after 100 cycles at 1 C (Figure 6). The high-frequency semicircle corresponds to the

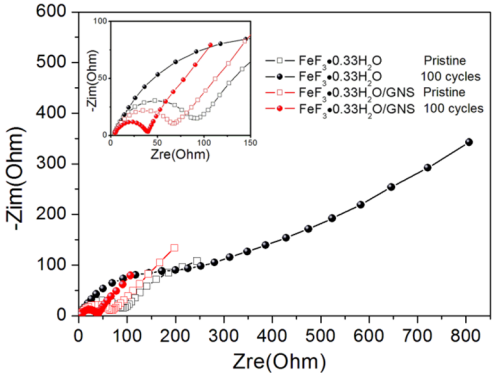

Figure 6. Nyquist plots of the $FeF_3{\cdot}0.33H_2O$ and $FeF_3{\cdot}0.33H_2O$/GNS cathodes before cycle and after 100 cycles at 1 C. Inset: an enlarged scale at high frequency.

charge-transfer resistance (R_{ct}); the inclined line can be attributed to the diffusion process of lithium ion within the electrode.[50,51] Nyquist plots of an unsupported $FeF_3{\cdot}0.33H_2O$ electrode showed depressed semicircles in the high and intermediate frequency region, indicating notable charge-transfer resistances of 86 and 147 Ω before and after 100 cycles, respectively. On the contrary, the values of R_{ct} for the $FeF_3{\cdot}0.33H_2O$/GNS electrode decrease after 100 cycles, suggesting that the $FeF_3{\cdot}0.33H_2O$/GNS electrode owns a high electron conductivity and a fast charge-transfer reaction for Li^+ insertion/extraction. The result is consistent with the cyclic performance. The slightly increased capacity can be attributed to further exfoliation of GNSs by the penetration of Li ions.[52,53] This exfoliation can expose new accessible active sites in GNSs, thus delivering an increased capacity over cycles. To our best knowledge, this $FeF_3{\cdot}0.33H_2O$/GNS hybrid exhibits the best performance in high-rate capacity and long cyclic stability to date, with a specific capacity of 74 mAh g^{-1} at 40 C and 115 mAh g^{-1} at 10 C after 250 cycles.

CONCLUSIONS

Herein, an *in situ* IL-assisted synthetic approach was presented to fabricate a novel $FeF_3{\cdot}0.33H_2O$/GNS hybrid nanostructure. The resulting high capacity and outstanding high-rate cyclic performance were ascribed to the synergies between tunnel-type $FeF_3{\cdot}0.33H_2O$ and graphene and their robust hybrid structure. The flexible GNSs built up interleaved electron transfer highways and served as an "elastic confinement" to anchor $FeF_3{\cdot}0.33H_2O$ particles and restrain the detachment and agglomeration of the $FeF_3{\cdot}0.33H_2O$ nanoparticles. Simultaneously, the $FeF_3{\cdot}0.33H_2O$ particles deter the restacking of GNSs. The $FeF_3{\cdot}0.33H_2O$/GNS hybrid cathode exhibits a high specific capacity of 74 mAh g^{-1} at 8 A g^{-1} (40 C) and rate cycling performance of 115 mAh g^{-1} after 250 cycles (10 C). The superior electrochemical performance of $FeF_3{\cdot}0.33H_2O$/GNS hybrids as a LIB cathode makes such hybrid materials a promising cathode material for the development of high power and energy density lithium batteries. The strategy of constructing $FeF_3{\cdot}0.33H_2O$/GNS hybrid nanostructures demonstrated in this work could be potentially extended to other graphene hybrids.

EXPERIMENTAL SECTION

Synthesis of the GNSs. We prepared GNSs by a chemical reduction method after the exfoliation of the natural flake graphite (96%, pursued from Qingdao Guyu Graphite Co., Ltd.).[19,48,54] The graphene preparation process involved two main steps: first, the natural flake graphite was oxidized by $KMnO_4$ (99.5%, pursued from Sinopharm Chemical Reagent Co., Ltd. without further purification) in a mixed acid solution at room temperature for 40 h to prepare the sticky graphene oxide using a modified Hummers methods; then, graphene oxide was reduced by $C_6H_6O_2$ (99%, pursued from Crystal Pure Industrial Co. Ltd. without further purification) by chemical method to gain the graphene.

Synthesis of $FeF_3{\cdot}0.33H_2O$/GNS Hybrid. We dispersed 50 mg of GNSs in 150 mL of alcohol by ultrasonication for 1 h. Then, 10 mL of [Bmim][BF_4] (99%, pursued from Centre for Green Chemistry and Catalysis, LICP, CAS.) was added to obtain a uniformly dispersed GNS solution. A 1 g portion of $Fe(NO_3)_3{\cdot}9H_2O$ (99.99%, pursued from Crystal Pure Industrial Co. Ltd. without further purification) was added into the obtained solution and then stirred for 30 min. After continuously stirring at 80 °C for 8 h, we washed the resulting product five times with acetone and dried under vacuum conditions at 80 °C overnight. Noticeably, a prior vacuum treatment for removing a certain extent of hydration water was needed.[14−16] The synthetic procedure of bare $FeF_3{\cdot}0.33H_2O$ was just like the procedure of $FeF_3{\cdot}0.33H_2O$/GNS hybrid but without adding GNSs.

Material Characterizations. X-ray diffraction (Rigaku, monochromated Cu Kα radiation 50 mA, 45 kV with a step size of 0.02°), transmission electron microscopy (FTI, Tecnai F20, 300 kV), and micro-Raman spectroscopy (HR800, 632.8 nm laser) were applied to characterize the detailed structure and morphology information of the materials. N_2 adsorption/desorption isotherms were measured by using an ASAP 2020 (Micromeritics) instrument. The carbon content in the hybrid was measured by a carbon−sulfur elements determinator (Baoying technology CS-206).

Cell Fabrication and Electrochemical Characterizations. The electrochemical properties of the $FeF_3{\cdot}0.33H_2O$/GNS hybrid and bare $FeF_3{\cdot}0.33H_2O$ particles were measured by the galvanostatic charge/discharge technique as cathode materials in LIBs.[55,56] The electrode slurry was fabricated by mixing active materials with polyvinylidene fluoride (PVDF was dissolved in *N*-methyl-2-pyrrolidone (NMP) with

a content of 10 wt %) as a binder and carbon black as a conductive agent with a weight ratio of 8:1:1. The obtained slurry was coated by a doctor-balding method onto a cleaned aluminum foil. Then, the electrodes were cut into discs with a diameter of 14 mm and dried at 120 °C overnight under a vacuum. The coin type (CR-2025) test cells were assembled in an argon-filled glovebox (Mbraun, H_2O <0.1 ppm, O_2 <1 ppm) using 1 M $LiPF_6$ in diethyl carbonate, ethylene carbonate, and ethylmethyl carbonate (EC/EMC/DMC, 1:1:1 in vol) as an electrolyte, two pieces of porous polypropylene films (Celgard 2400) as the separator, and metallic lithium as the counter/reference electrode. All the as-prepared cells were stabilized for 12 h before measurements. Over a voltage range of 1.7−4.5 V (vs Li^+/Li), the discharge/charge measurements were carried out by using a Neware (Shenzhen Neware Electronic Co., China) battery test system at various current rates (1 C is equivalent to 200 mA g^{-1}). Electrical impedance spectroscopy (EIS) measurements were carried out using an electrochemical workstation (Princeton Applied Research PAR-STAT 2273 advanced electrochemical system) over the frequency range between 1 MHz and 100 mHz with the amplitude of an ac signal of 10 mV. All the EIS measurements were carried out at the open circuit voltage (~3.5 V) of the cells in order to avoid the influence of the state of charge.

■ ASSOCIATED CONTENT

Supporting Information

TEM morphology of $FeF_3{\cdot}0.33H_2O$ nanoparticles free of graphene and nitrogen sorption isotherms and corresponding pore size distribution of the $FeF_3{\cdot}0.33H_2O$/GNS hybrid. This material is available free of charge via the Internet at http://pubs.acs.org.

■ AUTHOR INFORMATION

Corresponding Author

*E-mail: keningsun@yahoo.com.cn. Phone: (+86) 045186412153. Fax: (+86) 045186412153.

Author Contributions

All authors have given approval to the final version of the manuscript.

Notes

The authors declare no competing financial interest.

■ ACKNOWLEDGMENTS

This work was supported by State Key Laboratory of Urban Water Resource and Environment, Harbin Institute of Technology, (No. 2013TS08).

■ REFERENCES

(1) Tarascon, J. M.; Armand, M. *Nature* **2001**, *414*, 359−367.
(2) Armand, M.; Tarascon, J. M. *Nature* **2008**, *451*, 652−657.
(3) Cho, J.; Kim, Y. J.; Park, B. *Chem. Mater.* **2000**, *12*, 3788−3791.
(4) Sun, C. W.; Rajasekhara, S.; Goodenough, J. B.; Zhou, F. *J. Am. Chem. Soc.* **2011**, *133*, 2132−2135.
(5) Prosini, P. P.; Zane, D.; Pasquali, M. *Electrochim. Acta* **2001**, *46*, 3517−3523.
(6) Badway, F.; Cosandey, F.; Pereira, N.; Amatucci, G. G. *J. Electrochem. Soc.* **2003**, *150*, A1318−A1327.
(7) Badway, F.; Pereira, N.; Cosandey, F.; Amatucci, G. G. *J. Electrochem. Soc.* **2003**, *150*, A1209−A1218.
(8) Arai, H.; Okada, S.; Sakurai, Y.; Yamaki, J. *J. Power Sources* **1997**, *68*, 716−719.
(9) Li, T.; Li, L.; Cao, Y. L.; Ai, X. P.; Yang, H. X. *J. Phys. Chem. C* **2010**, *114*, 3190−3195.
(10) Kim, S. W.; Seo, D. H.; Gwon, H.; Kim, J.; Kang, K. *Adv. Mater.* **2010**, *22*, 5260−5264.
(11) Liu, L.; Zhou, M.; Yi, L. H.; Guo, H. P.; Tan, J. L.; Shu, H. B.; Yang, X. K.; Yang, Z. H.; Wang, X. Y. *J. Mater. Chem.* **2012**, *22*, 17539−17550.
(12) Li, L. S; Meng, F.; Jin, S. *Nano Lett.* **2012**, *12*, 6030−6037.
(13) Ma, D. L.; Cao, Z. Y.; Wang, H. G.; Huang, X. L.; Wang, L. M.; Zhang, X. B. *Energy Environ. Sci.* **2012**, *5*, 8538−8542.
(14) Li, C. L.; Gu, L.; Tsukimoto, S.; van Aken, P. A.; Maier, J. *Adv. Mater.* **2010**, *22*, 3650−3654.
(15) Li, C. L.; Gu, L.; Tong, J. W.; Tsukimoto, S.; Maier, J. *Adv. Funct. Mater.* **2011**, *21*, 1391−1397.
(16) Li, C. L.; Gu, L.; Tong, J. W.; Maier, J. *ACS Nano* **2011**, *5*, 2930−2938.
(17) Geim, A. K.; Novoselov, K. S. *Nat. Mater.* **2007**, *6*, 183−191.
(18) Wang, D. H.; Choi, D. W.; Li, J.; Yang, Z. G.; Nie, Z. M.; Kou, R.; Hu, D. H.; Wang, C. M.; Saraf, L. V.; Zhang, J. G. *ACS Nano* **2009**, *3*, 907−914.
(19) Zhou, G. M.; Wang, D. W.; Li, F.; Zhang, L. L.; Li, N.; Wu, Z. S.; Wen, L.; Lu, G. Q.; Cheng, H. M. *Chem. Mater.* **2010**, *22*, 5306−5313.
(20) Wu, Z. S.; Ren, W. C.; Wen, L.; Gao, L. B; Zhao, J. P.; Chen, Z. P.; Zhou, G. M.; Li, F.; Cheng, H. M. *ACS Nano* **2010**, *4*, 3187−3194.
(21) Peng, C. X.; Chen, B. D.; Qin, Y.; Yang, S. H.; Li, C. Z.; Zuo, Y. H.; Liu, S. Y.; Yang, J. H. *ACS Nano* **2012**, *6*, 1074−1081.
(22) Chang, K.; Chen, W. X. *ACS Nano* **2011**, *5*, 4720−4728.
(23) Peigney, A.; Laurent, C.; Flahaut, E.; Bacsa, R. R.; Rousset, A. *Carbon* **2001**, *39*, 507−514.
(24) Zhao, X.; Hayner, C. M.; Kung, M. C.; Kung, H. H. *Chem. Commun.* **2012**, *48*, 9909−9911.
(25) Liu, J.; Wan, Y. L.; Liu, W.; Ma, Z. S.; Ji, S. M.; Wang, J. B.; Zhou, Y. C.; Hodgson, P.; Li, Y. C. *J. Mater. Chem. A* **2013**, *1*, 1969−1975.
(26) Kim, T.; Lee, H.; Kim, J.; Suh, K. S. *ACS Nano* **2010**, *4*, 1612−1618.
(27) Acik, M.; Dreyer, D. R.; Bielawski, C. W.; Chabal, Y. J. *J. Phys. Chem. C* **2012**, *116*, 7867−7873.
(28) Fukushima, T.; Aida, T. *Chem.—Eur. J.* **2007**, *13*, 5048−5058.
(29) Liu, N.; Luo, F.; Wu, H. X.; Liu, Y. H.; Zhang, C.; Chen, J. *Adv. Funct. Mater.* **2008**, *18*, 1518−1525.
(30) Jacob, D. S.; Bitton, L.; Grinblat, J.; Felner, I.; Koltypin, Y.; Gedanken, A. *Chem. Mater.* **2006**, *18*, 3162−3168.
(31) Miao, Z. J.; Liu, Z. M.; Ding, K. L.; Han, B. X.; Miao, S. D.; An, G. M. *Nanotechnology* **2006**, *18*, 125605-1−125605-5.
(32) Shen, L. F.; Yuan, C. Z.; Luo, H. J.; Zhang, X. G.; Yang, S. D.; Lu, X. J. *Nanoscale* **2011**, *3*, 572−574.
(33) Xu, C. H.; Sun, J.; Gao, L. *J. Mater. Chem.* **2012**, *22*, 975−979.
(34) Chen, W. F.; Li, S. R.; Chen, C. H.; Yan, L. F. *Adv. Mater.* **2011**, *23*, 5679−5683.
(35) Tuinstra, F.; Koenig, J. L. *J. Chem. Phys.* **1970**, *53*, 1126−1130.
(36) Ferrari, A. C.; Meyer, J. C.; Scardaci, V.; Casiraghi, C.; Lazzeri, M.; Mauri, F.; Piscanec, S.; Jiang, D.; Novoselov, K. S.; Roth, S.; Geim, A. K. *Phys. Rev. Lett.* **2006**, *97*, 187401-1−187401-4.
(37) Kudin, K. N.; Ozbas, B.; Schniepp, H. C.; Prud'homme, R. K.; Aksay, I. A.; Car, R. *Nano Lett.* **2008**, *8*, 36−41.
(38) Dresselhaus, M. S.; Jorio, A.; Hofmann, M.; Dresselhaus, G.; Saito, R. *Nano Lett.* **2008**, *8*, 2277−2282.
(39) Mohiuddin, T. M. G.; Lombardo, A.; Nair, R. R.; Bonetti, A.; Savini, G.; Jalil, R.; Bonini, N.; Basko, D. M.; Galiotis, C.; Marzari, N.; Novoselov, K. S.; Geim, A. K.; Ferrari, A. C. *Phys. Rev. B* **2009**, *79*, 205433-1−205433-8.
(40) Li, B. J.; Cao, H. Q.; Zhang, J. X.; Qu, M. Z.; Lian, F.; Kong, X. H. *J. Mater. Chem.* **2012**, *22*, 2851−2854.
(41) Zhou, J. S.; Song, H. H.; Ma, L. L.; Chen, X. H. *RSC Adv.* **2011**, *1*, 782−791.
(42) Luo, B.; Fang, Y.; Wang, B.; Zhou, J. S.; Song, H. H.; Zhi, L. J. *Energy Environ. Sci.* **2012**, *5*, 5226−5230.
(43) Sun, Y. M.; Hu, X. L.; Luo, W.; Huang, Y. H. *ACS Nano* **2011**, *5*, 7100−7107.
(44) Liu, C. G.; Yu, Z. N.; Neff, D.; Zhamu, A.; Jang, B. Z. *Nano Lett.* **2010**, *10*, 4863−4868.

(45) Yamakawa, N.; Jiang, M.; Key, B.; Grey, C. P. *J. Am. Chem. Soc.* **2009**, *131*, 10525−10536.
(46) Lee, S. W.; Yabuuchi, N.; Gallant, B. M.; Chen, S.; Kim, B. S.; Hammond, P. T.; Shao-Horn, Y. *Nat. Nanotechnol.* **2010**, *5*, 531−537.
(47) Behera, S. K. *Chem. Commun.* **2011**, *47*, 10371−10373.
(48) Zhu, X. J.; Zhu, Y. W.; Murali, S.; Stollers, M. D.; Ruoff, R. S. *ACS Nano* **2011**, *5*, 3333−3338.
(49) Chen, Y.; Song, B. H.; Tang, X. S.; Lu, L.; Xue, J. M. *J. Mater. Chem.* **2012**, *22*, 17656−17662.
(50) Chou, S. L.; Wang, J. Z.; Choucair, M.; Liu, H. K.; Stride, J. A.; Dou, S. X. *Electrochem. Commun.* **2010**, *12*, 303−306.
(51) Xiao, J.; Wang, X. J.; Yang, X. Q.; Xun, S. D.; Liu, G.; Koech, P. K.; Liu, J.; Lemmon, J. P. *Adv. Funct. Mater.* **2011**, *21*, 2840−2846.
(52) Wang, J. Z.; Manga, K. K.; Bao, Q. L.; Loh, K. P. *J. Am. Chem. Soc.* **2011**, *133*, 8888−8891.
(53) Chen, Y.; Song, B. H.; Tang, X. H.; Lu, L.; Xue, J. M. *J. Mater. Chem.* **2012**, *22*, 17656−17662.
(54) Hummers, W. S.; Offeman, R. E. *J. Am. Chem. Soc.* **1958**, *80*, 1339−1339.
(55) Liu, Z. M.; Zhang, N. Q.; Sun, K. N. *J. Mater. Chem.* **2012**, *22*, 11688−11693.
(56) Yang, T. Y.; Zhang, N. Q.; Sun, K. N. *Electrochim. Acta* **2011**, *56*, 4058−4064.